

Missing Fine Details in Images: Last Seen in High Frequencies

Tejaswini Medi¹ Hsien-Yi Wang^{1,3} Arianna Rampini² Margret Keuper^{1,3}

¹University of Mannheim, Germany, ²Autodesk AI Lab, ³MPI for Informatics, Saarland Informatics Campus
tejaswini.medi@uni-mannheim.de

Abstract

Latent generative models have shown remarkable progress in high-fidelity image synthesis, typically using a two-stage training process that involves compressing images into latent embeddings via learned tokenizers in the first stage. The quality of generation strongly depends on how expressive and well-optimized these latent embeddings are. While various methods have been proposed to learn effective latent representations, generated images often lack realism, particularly in textured regions with sharp transitions, due to loss of fine details governed by high frequencies. We conduct a detailed frequency decomposition of existing state-of-the-art (SOTA) latent tokenizers and show that conventional objectives inherently prioritize low-frequency reconstruction, often at the expense of high-frequency fidelity. Our analysis reveals these latent tokenizers exhibit a bias toward low-frequency information during optimization, leading to over-smoothed outputs and visual artifacts that diminish perceptual quality. To address this, we propose a wavelet-based, frequency-aware variational autoencoder (FA-VAE) framework that explicitly decouples the optimization of low- and high-frequency components. This decoupling enables improved reconstruction of fine textures while preserving global structure. Moreover, we integrate our frequency-preserving latent embeddings into a SOTA latent diffusion model, resulting in sharper and more realistic image generation. Our approach bridges the fidelity gap in current latent tokenizers and emphasizes the importance of frequency-aware optimization for realistic image synthesis, with broader implications for applications in content creation, neural rendering, and medical imaging.

Introduction

Latent generative modeling (Blattmann et al. 2023; Dong et al. 2024; Luo et al. 2024; Zhou, Wang, and Zhang 2024) has emerged as a cornerstone of modern content creation, with recent advances demonstrating remarkable capabilities in synthesizing high-fidelity visual content. These models typically operate in compressed latent spaces learned via autoencoders such as VAEs (Kingma and Welling 2013; Li et al. 2024a), where generation quality is directly influenced by the expressiveness of the latent embeddings. While increasing latent dimensionality can enhance representational power, this often leads to diminishing visual out-

Copyright © 2026, Association for the Advancement of Artificial Intelligence (www.aaai.org). All rights reserved.

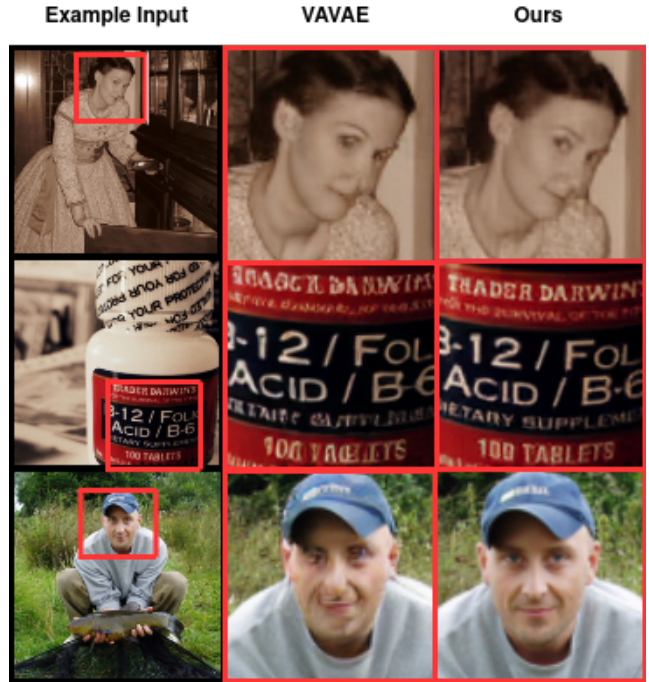


Figure 1: Visual comparison of reconstructions. From left to right: original image, VAVAE reconstruction, and our approach. The highlighted regions emphasize areas rich in textures, edges, and text. Our method better preserves high-frequency details and sharp structures, resulting in reconstructions visually closer to the input.

puts and increased computational cost. VAVAE (Yao, Yang, and Wang 2025) addresses this by aligning the latent space with pre-trained vision foundation models to improve convergence and generative realism. However, despite such improvements, generated outputs often lack sharp textures and fine details, particularly in regions dominated by the high-frequency information such as text on images. This limits perceptual realism and results in overly smooth reconstructions. Prior works (Phung, Dao, and Tran 2023; Li et al. 2024b; Guth et al. 2022) have explored architectural and spectral enhancements to inject high-frequency signals, but a systematic frequency-level analysis of how these current latent embeddings influence reconstruction quality, especially

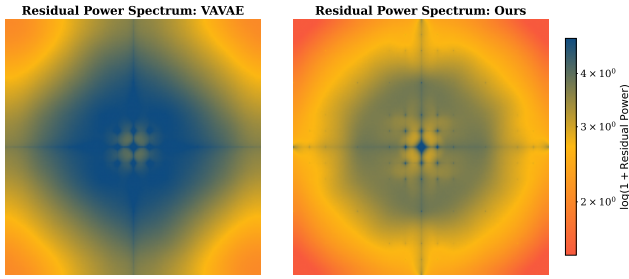


Figure 2: Residual power spectra averaged over 50k ImageNet validation images, comparing reconstruction errors (input minus reconstruction) of VAVAE and our method. The log-scaled spectra show that VAVAE exhibits higher residual energy across the frequency spectrum, particularly in high-frequency regions. In contrast, our method significantly reduces reconstruction residual energy, indicating better preservation of fine details and textures.

in differentiating low- vs. high-frequency information remains absent.

In this work, we conduct a comprehensive frequency-based analysis of the reconstruction behavior of state-of-the-art latent embeddings used in generative pipelines (Yao, Yang, and Wang 2025; Li et al. 2024a; Tian et al. 2024; Xie et al. 2024, 2025), focusing on latent diffusion and autoregressive models, which represent the current forefront of high-quality visual generation. These models typically follow a two-stage pipeline: (1) learning quantized or non-quantized latent embeddings using a VAE variant, and (2) training a probabilistic generative model in the latent space. Our analysis reveals a consistent bias: while low-frequency components are well reconstructed, high-frequency signals such as textures and fine structures are poorly preserved. This low frequency bias over high frequencies in optimization contributes significantly to perceptual degradation.

To address this fidelity gap, we propose a novel **Frequency-aware VAE (FA-VAE)** framework that explicitly decouples and separately optimizes low- and high-frequency components via wavelet decomposition. Our method learns distinct latent embeddings for frequency subbands and later fuses them into a unified latent space representation. This simple design allows for better preservation of both global structure and fine details. Figure 1 presents a visual comparison between our method and the recent state-of-the-art VAVAE, highlighting improved preservation of fine details and sharp structures. Complementarily, Figure 2 quantifies reconstruction quality in the frequency domain using the average residual power spectrum of reconstruction errors computed with respect to input over 50K ImageNet (Deng et al. 2009) validation images. Our method consistently exhibits lower residual energy across both low (middle of spectrum) and high (corners of the spectrum) frequency bands, with a particularly notable reduction in high-frequency at corners of the power spectrum. This indicates more faithful reconstructions over the frequency spectrum, directly contributing to the enhanced perceptual quality observed in Figure 1. Finally, we integrate our frequency aware latent embeddings into a lightweight latent diffusion

model (**LightningDiT**, based on VAVAE), to showcase our frequency-aware embeddings enable sharper, more realistic generations.

Our main contributions are summarized as follows:

- ✓ We provide a frequency-based analysis of latent embeddings used in latent generative pipelines, showing that existing VAE variants disproportionately emphasize low-frequency components at the expense of fine detail.
- ✓ We introduce **FA-VAE**, a frequency-aware VAE framework that decouples optimization of low- and high-frequency subbands using wavelet decomposition, resulting in frequency aware expressive latent representations.
- ✓ We integrate FA-VAE embedding space into a diffusion pipeline (LightningDiT), demonstrating superior generation quality and perceptual fidelity across ImageNet, underscoring the role of frequency-aware modeling in high-fidelity synthesis.

Related Work

Latent Embeddings for Image Generation

Latent embeddings or tokenizers are widely used to represent compressed, high-dimensional visual data and enable efficient generation. Encoder–Decoder frameworks such as VAEs (Kingma and Welling 2013) and their variants form the foundation for learning these latent representations, which are vital to many latent generative models. Notably, Latent Diffusion Models (LDMs) (Rombach et al. 2022) operate over learned latent embeddings to facilitate high-quality synthesis, highlighting the importance of effective latent space modeling. Discrete tokenization techniques, such as VQ-VAE (Van Den Oord, Vinyals et al. 2017; Medi et al. 2024b), convert images to code sequences that can be effectively modeled by transformers. VQGAN (Esser et al. 2021) further improves this framework by incorporating adversarial losses to learn perceptually meaningful tokens, while RQ-VAE (Lee et al. 2022) enhances expressiveness of embeddings via stacked residual quantizers. Recent methods like TiTok (Yu et al. 2024a), FlexTok (Bachmann et al. 2025), and OneDPiece (Miwa et al. 2025) explore compact and adaptive tokenization strategies, aiming for better compression and controllable generation quality.

To enhance reconstruction quality of latent embeddings, hierarchical and regularized latent models have been proposed. NVAE (Vahdat and Kautz 2020) introduces spectral regularization within residual hierarchies for stable training, while HQ-VAE (Takida et al. 2023) and VAR (Tian et al. 2024) use multi-scale vector quantization to better model local and global structure. EQ-VAE (Kouzelis et al. 2025) imposes equivariance constraints for robustness to geometric changes. Additionally, frequency-aware losses such as fourier-based regularization (Björk, Myhre, and Johansen 2022) and scale-equivariant decoding (Skorokhodov et al. 2025) have been used to control the spectral properties of the latent reconstructions. A parallel direction focuses on aligning latent spaces with external vision encoders.

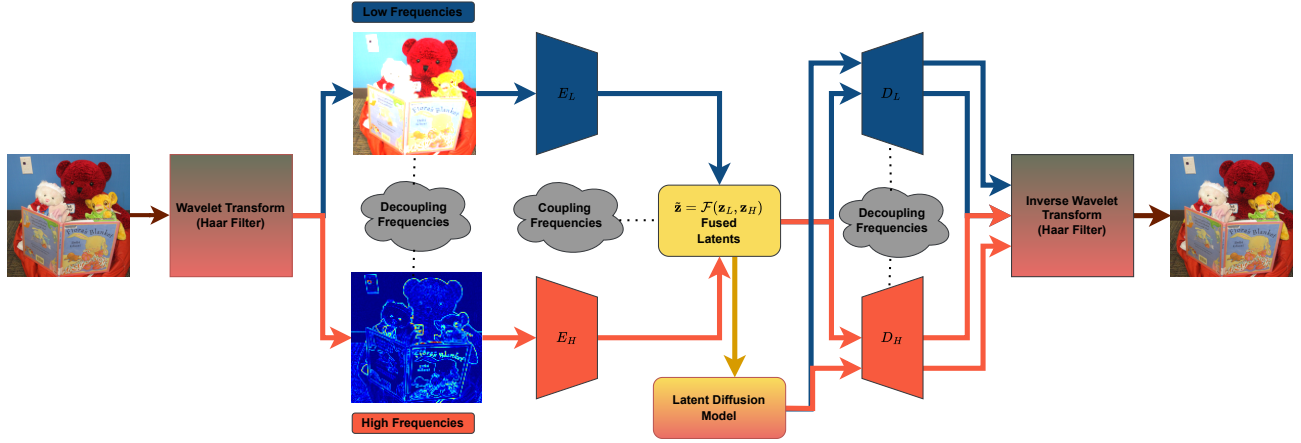


Figure 3: Overview of our proposed frequency-aware VAE framework (FA-VAE). An input image is decomposed into low- and high-frequency representations using a wavelet transform. Each frequency band is decoupled, encoded and decoded separately to learn dedicated latent embeddings, which are then coupled and passed through an inverse wavelet transform to reconstruct the image. These enriched embeddings are subsequently used in a latent diffusion model to improve generation fidelity, particularly preserving fine details.

REPA (Yu et al. 2024b) introduces denoising-time regularization based on foundation model features to accelerate convergence. VA-VAE (Yao, Yang, and Wang 2025) builds on this by jointly aligning tokenizer latents with pretrained features and optimizing for downstream generation quality. ReaLS (Xu et al. 2025) introduces semantic priors directly into the latent space to improve representation capacity. Our work builds on VA-VAE but identifies that such alignment alone does not sufficiently preserve high frequency details. We propose an explicit decoupling and optimization of low- and high-frequencies during tokenization, leading to improved fidelity.

High-Frequency Information in Image Synthesis

High-frequency content is essential for perceptual realism but challenging to reconstruct, particularly for diffusion-based models. Prior analyses show that frequency components are not reconstructed uniformly across the denoising trajectory (Yang et al. 2023), resulting in a loss of textures and sharp structures. To address this, various frequency-aware approaches have been developed across generative paradigms. In GANs, SWAGAN (Gal et al. 2021) and WaveFill (Yu et al. 2021) integrate wavelet transforms into their architectures to improve generation fidelity. Focal frequency loss (Jiang et al. 2021) and WINE (Kim, Moon, and Park 2025) address frequency imbalance by reweighting reconstruction errors and correcting low-frequency bias in inversion, respectively.

Diffusion models have incorporated frequency priors at both training and inference time. WaveDiff (Phung, Dao, and Tran 2023), Spatial-Frequency UNet (Yuan et al. 2023), and Spectral Diffusion (Yang et al. 2023) integrate wavelet-domain frequency components or gating mechanisms into the network to better optimize the spectral content. Training-free techniques like DiffuseHigh (Kim et al. 2025) and frequency aggregation (Qian et al. 2024) inject wavelet-based frequency priors during inference for improved detail preser-

vation. Additional strategies include replacing convolutions with filtered variants in FouriScale (Huang et al. 2024), and autoregressive frequency modeling in NFIG (Huang et al. 2025). Adaptations also exist for domain-specific tasks such as high-resolution (Zhang et al. 2025), underwater (Zhao et al. 2024), or low-light image generation (Jiang et al. 2023). Beyond images, wavelet representations have further proven useful in 3D generation with diffusion and autoregressive models (Hui et al. 2024; Medi et al. 2024a), suggesting the utility of wavelet decompositions as a general tool for capturing fine-scale structure across visual modalities. While effective, these approaches typically introduce additional architectural components or post-processing steps to compensate for frequency degradation. In contrast, our method addresses the root cause by improving frequency preservation at the latent representation level. By modeling and optimizing frequency subbands (low and high) separately during tokenization, we improve the frequency aware expressivity in the latent embeddings. These latent embeddings improve both reconstruction fidelity and downstream synthesis quality when integrated with latent generative pipeline without requiring any architectural changes at generation time.

Method

In this section, we present three key contributions. First, we conduct a detailed frequency analysis of latent embeddings commonly used in high-fidelity image generation. Second, we propose **FA-VAE**, a novel framework that decouples and independently optimizes low- and high-frequency components of the embeddings. Third, we introduce a simple fusion strategy to unify both components into a single latent representation, which is integrated into the LightningDiT pipeline (Yao, Yang, and Wang 2025), resulting in improved image generation via frequency-aware latent modeling. An overview of our framework is shown in Figure 3.

Frequency Evaluation of Latent Embeddings

In most latent generative models, the first stage of training includes Variational Autoencoders (VAEs) or their other visual tokenizer variants, aiming to learn compact latent embeddings $\mathbf{z} \in \mathcal{Z}$ that capture the underlying structure of the input data $\mathbf{x} \in \mathcal{X}$. A common measure of representational quality is the reconstruction error computed via the mean squared error (MSE) or ℓ_2 -loss:

$$\mathcal{L}_{\text{rec}} = \|\mathbf{x} - \hat{\mathbf{x}}\|_2^2,$$

where $\hat{\mathbf{x}} = D(E(\mathbf{x}))$ is the reconstruction obtained by encoding \mathbf{x} to a latent representation $\mathbf{z} = E(\mathbf{x})$, followed by decoding with decoder D to obtain reconstruction $\hat{\mathbf{x}}$.

Similarly, To assess the fidelity of reconstructions across low and high frequency bands, we employ a *discrete wavelet transform* (DWT) using Haar filter to decompose both the input and its reconstruction into respective low- and high-frequency representations. Let $\mathcal{W}(\cdot)$ denote the wavelet decomposition operator:

$$\mathcal{W}(\mathbf{x}) = (\mathbf{x}_L, \mathbf{x}_H), \quad \mathcal{W}(\hat{\mathbf{x}}) = (\hat{\mathbf{x}}_L, \hat{\mathbf{x}}_H),$$

where \mathbf{x}_L and $\hat{\mathbf{x}}_L$ correspond to the low-frequency (approximation) representations, and \mathbf{x}_H , $\hat{\mathbf{x}}_H$ correspond to the high-frequency (detail) representations. We then compute frequency-specific reconstruction losses:

$$\mathcal{L}_L = \|\mathbf{x}_L - \hat{\mathbf{x}}_L\|_2^2, \quad \mathcal{L}_H = \|\mathbf{x}_H - \hat{\mathbf{x}}_H\|_2^2.$$

This evaluation provides insight into the frequency fidelity of latent embeddings, measuring their ability to capture both low and high frequency information from input representation.

Beyond pixel-wise reconstruction loss, we also assess perceptual quality using the Learned Perceptual Image Patch Similarity (LPIPS) metric (Zhang et al. 2018), $\mathcal{L}_{\text{LPIPS}} = \text{LPIPS}(\mathbf{x}, \hat{\mathbf{x}})$. To further quantify the overall quality of the latent reconstructions, we compute the reconstruction Fréchet Inception Distance (rFID) (Heusel et al. 2017) which compares the distribution of original and reconstructed images in the feature space of a pretrained Inception network (Szegedy et al. 2016):

$$\text{rFID} = \|\mu_{\mathbf{x}} - \mu_{\hat{\mathbf{x}}}\|_2^2 + \text{Tr} \left(\Sigma_{\mathbf{x}} + \Sigma_{\hat{\mathbf{x}}} - 2(\Sigma_{\mathbf{x}}\Sigma_{\hat{\mathbf{x}}})^{1/2} \right),$$

where $(\mu_{\mathbf{x}}, \Sigma_{\mathbf{x}})$ and $(\mu_{\hat{\mathbf{x}}}, \Sigma_{\hat{\mathbf{x}}})$ are the means and covariances of Inception features extracted from the original and reconstructed image sets, respectively.

Together, the frequency-aware losses $(\mathcal{L}_L, \mathcal{L}_H)$, perceptual similarity $\mathcal{L}_{\text{LPIPS}}$, and distributional alignment via rFID provide a comprehensive evaluation of the reconstruction quality and frequency fidelity of latent embeddings.

Frequency-Aware VAE (FA-VAE)

To enhance the fidelity of latent embeddings, we extend the standard VAE formulation by decoupling the input image into low- and high-frequency components, which are then learned independently. Given an input image $\mathbf{x} \in \mathcal{X}$, we apply a discrete wavelet transform $\mathcal{W}(\cdot)$ to obtain:

$$\mathcal{W}(\mathbf{x}) = (\mathbf{x}_L, \mathbf{x}_H),$$

where \mathbf{x}_L and \mathbf{x}_H denote the low- and high-frequency representations, respectively. We use the Haar filter for wavelet transformation, and apply the normalization strategy proposed in (Mulcahy 1997) to normalize both low and high frequency components. We employ separate encoder-decoder pairs (E_L, D_L) and (E_H, D_H) to learn frequency-specific latent embeddings:

$$\mathbf{z}_L = E_L(\mathbf{x}_L), \quad \mathbf{z}_H = E_H(\mathbf{x}_H).$$

Low-Frequency Objective. To learn low-frequency latent embeddings, we adopt a VA-VAE-style objective (Yao, Yang, and Wang 2025), incorporating a vision foundation alignment loss $\mathcal{L}_{\text{VF}}^L$ (Yao, Yang, and Wang 2025), adversarial regularization $\mathcal{L}_{\text{GAN}}^L$ inspired by VQGAN (Esser et al. 2021), and an additional perceptual loss $\mathcal{L}_{\text{LPIPS}}^L$ (Zhang et al. 2018) to improve visual quality. The total low-frequency objective is defined as:

$$\mathcal{L}_{\text{low}} = \mathcal{L}_{\text{rec}}^L + \beta \cdot \mathcal{L}_{\text{KL}}^L + \lambda_{\text{VF}} \cdot \mathcal{L}_{\text{VF}}^L + \lambda_{\text{GAN}} \cdot \mathcal{L}_{\text{GAN}}^L + \lambda_{\text{LPIPS}} \cdot \mathcal{L}_{\text{LPIPS}}^L$$

where:

$$\begin{aligned} \mathcal{L}_{\text{rec}}^L &= \mathbb{E}_{q(\mathbf{z}_L | \mathbf{x}_L)} \left[\|\mathbf{x}_L - D_L(\mathbf{z}_L)\|_2^2 \right], \\ \mathcal{L}_{\text{KL}}^L &= D_{\text{KL}}(q(\mathbf{z}_L | \mathbf{x}_L) \| p(\mathbf{z}_L)), \end{aligned}$$

with $q(\mathbf{z}_L | \mathbf{x}_L)$ being the encoder’s approximate posterior and $p(\mathbf{z}_L) \sim \mathcal{N}(\mathbf{0}, \mathbf{I})$, the standard Gaussian prior.

The vision foundation loss $\mathcal{L}_{\text{VF}}^L$ aligns the latent codes with the feature space of a pretrained foundation model (e.g., DINOv2 (Oquab et al. 2023)). The adversarial loss $\mathcal{L}_{\text{GAN}}^L$ introduces a discriminator to distinguish real from reconstructed low-frequency inputs. Finally, the perceptual loss $\mathcal{L}_{\text{LPIPS}}^L$ encourages perceptual similarity between input and reconstruction using features from a pretrained Inception network (Szegedy et al. 2016). All these loss components are commonly used in modern VAE frameworks.

High-Frequency Objective. In contrast, high-frequency components are trained without supervision from pretrained models, as they tend to be biased toward low-frequency content. We use a lightweight VAE objective focused on reconstructing fine-scale details, along with adversarial regularization:

$$\begin{aligned} \mathcal{L}_{\text{high}} &= \mathcal{L}_{\text{rec}}^H + \beta \cdot \mathcal{L}_{\text{KL}}^H + \mathcal{L}_{\text{GAN}}^H, \\ \mathcal{L}_{\text{rec}}^H &= \mathbb{E}_{q(\mathbf{z}_H | \mathbf{x}_H)} \left[\|\mathbf{x}_H - D_H(\mathbf{z}_H)\|_1 \right], \\ \mathcal{L}_{\text{KL}}^H &= D_{\text{KL}}(q(\mathbf{z}_H | \mathbf{x}_H) \| p(\mathbf{z}_H)) \end{aligned}$$

Inference. At inference time, both decoders are used to reconstruct the respective frequency bands, and the final image is synthesized via inverse wavelet transform:

$$\hat{\mathbf{x}}_L = D_L(\mathbf{z}_L), \quad \hat{\mathbf{x}}_H = D_H(\mathbf{z}_H), \quad \hat{\mathbf{x}} = \mathcal{W}^{-1}(\hat{\mathbf{x}}_L, \hat{\mathbf{x}}_H).$$

This frequency-aware latent representation learning via FA-VAE yields more expressive embeddings by preserving both coarse structure and fine details across the full spectrum of spatial frequencies.

Model (Tokenizer)	Tokenizer Config	Recon. Loss	Low Freq. Loss	High Freq. Loss	LPIPS	rFID
DC-AE	f32c32	0.0194	0.0484	0.0097	0.1580	0.7450
DC-AE	f64c128	0.0207	0.0527	0.0100	0.1667	0.7623
DC-AE	f128c512	0.0225	0.0581	0.0106	0.1805	0.7912
SD-VAE	f16c16	0.0180	0.0422	0.0100	0.1743	0.6213
KL-VAE	f16c16	0.0148	0.0326	0.0089	0.1355	0.5318
MS-VQ-VAE	f16c32v4096	0.0195	0.0549	0.0076	0.1890	0.6981
RQ-VAE	f32c256v16384	0.0416	0.1219	0.0149	0.2712	0.9095
TiTok-VQ-VAE	f256x2c64v8192	0.0226	0.0561	0.0114	0.2082	0.7550
TiTok-VQ-VAE	f256x4c64v8192	0.0339	0.0947	0.0137	0.2657	0.8823
TiTok-VQ-VAE	f256x8c64v8192	0.0450	0.1344	0.0152	0.2949	0.9416
TiTok-VAE	f256x1c16	0.0332	0.0923	0.0134	0.2232	0.8640
TiTok-VAE	f256x2c16	0.0461	0.1380	0.0155	0.2682	0.9187
TiTok-VAE	f256x4c16	0.0617	0.1961	0.0170	0.3182	0.9761
VQ-VAE	f16c256v1024	0.0492	0.1478	0.0163	0.3064	0.9102
VQ-VAE	f16c256v16384	0.0438	0.1262	0.0164	0.2784	0.8826
VA-VAE	f16c32	0.0105	0.0200	0.0074	0.0975	0.4884
FA-VAE (Ours)	f16c32	0.0044	0.0114	0.0020	0.0940	0.4156

Table 1: Quantitative comparison of various latent tokenizers based on their reconstruction quality across multiple metrics. Tokenizer configurations are denoted as: **f** : latent spatial resolution, **c**: latent dimensionality, and **v**: vocabulary size in case of quantized models. Lower values indicate better performance.

Latent Fusion for Generative Modeling

To enable frequency-aware generation, we integrate the proposed FA-VAE into the recent latent diffusion model LightningDiT (Yao, Yang, and Wang 2025) by considering the learned low-frequency embedding $\mathbf{z}_L \sim q(\mathbf{z} | \mathbf{x})$ as the primary latent representation. To enrich this representation, we fuse it with a complementary high-frequency latent code \mathbf{z}_H , which is aligned to enhance the representational capacity of \mathbf{z}_L . The two embeddings are combined using a lightweight fusion function:

$$\tilde{\mathbf{z}} = \mathcal{F}(\mathbf{z}_L, \mathbf{z}_H),$$

where \mathcal{F} denotes a simple concatenation operation that preserves both spatial and semantic alignment between the frequency bands. The resulting fused latent embedding $\tilde{\mathbf{z}}$ retains global structural coherence from \mathbf{z}_L , while incorporating fine-scale details through \mathbf{z}_H . This design is fully modular and plug-and-play, allowing seamless integration into existing generative architectures without requiring modifications to the underlying model structure.

Experiments

In this section, we present comprehensive evaluations to support our proposed contributions. We first assess the reconstruction performance of various latent embedding tokenizers, including our FA-VAE, in both spatial and spectral domains. To evaluate their generative utility, we integrate the embeddings into standard image synthesis pipelines, comparing FA-VAE combined with LightningDiT (Yao, Yang, and Wang 2025). All experiments are conducted on ImageNet-1K (Deng et al. 2009) and use 50k ImageNet Validation samples for quantitative evaluations. Beyond visual quality, we also examine embedding fairness

across challenging ImageNet categories, comparing against VAAE, the best and recent baseline. Results show that our frequency-aware embeddings improve reconstruction fidelity and promote a more fair latent space, especially for structurally complex classes. Further implementation details of our experiments are provided in Appendix A.2.

Performance Evaluation of Latent Embeddings

To evaluate the reconstruction performance of latent embeddings in both the spatial and spectral (frequency) domains, we consider a range of widely adopted visual tokenizers commonly used in modern latent generative models. These tokenizers are based on different variants of autoencoding architectures, each aiming to learn compact and informative latent embedding representations of the input data distribution. For a comprehensive analysis, we include recent representative tokenizers based on standard Autoencoders (Chen et al. 2024), Variational Autoencoders (VAEs) (Rombach et al. 2022; Li et al. 2024a; Lee et al. 2022; Yu et al. 2024a; Yao, Yang, and Wang 2025), and Vector Quantized Autoencoders (VQ-VAEs) (Yu et al. 2024a; Esser et al. 2021; Tian et al. 2024). We also include our proposed FA-VAE, which explicitly incorporates frequency-awareness into the latent embedding learning process. This selection enables a fair comparison across diverse tokenization strategies with varying latent dimensionalities (**c**) and latent feature resolutions (**f**) as shown in Table 1 with diverse tokenization configurations. We use the metrics discussed in method section for our evaluation.

Our analysis in Table 1 reveals that KL-regularized VAE with well-designed parameterizations consistently outperform both traditional VAE and vector quantization (VQ-VAE) baselines across all reconstruction metrics. Also KL-



Figure 4: Generated Visualization of our proposed FA-VAE together with LightningDiT-XL trained on ImageNet 256×256 resolution.

regularized VAE show efficient reconstruction performance at much better compression rate with lower dimensionality. This improvement stems from the absence of quantization artifacts, which often degrade reconstruction quality in discrete latent spaces. Additionally, the effectiveness of KL-VAE is closely tied to the quality of their latent parameterization schemes. Notably, KL-VAE employed in recent autoregressive models (Chen et al. 2025), and VA-VAE (Yao, Yang, and Wang 2025) which further aligns its latent space with foundation models like DINOv2 (Oquab et al. 2023) achieve strong performance across low and high-frequency reconstruction, along with improved perceptual quality. However, these models still rely on a joint optimization of frequency components, which can lead to trade-offs and suboptimal detail preservation, especially in the high-frequency spectrum. In contrast, our proposed Frequency-Aware VAE (FA-VAE) builds on the VA-VAE framework by explicitly decoupling and modeling low- and high-frequency components in learning of the compact latent embeddings. This separation enables focused representation learning for each frequency band, leading to more precise reconstructions of both global structures and fine details. FA-VAE achieves the best overall performance across all evaluated metrics nearly halving the reconstruction loss of the strongest baseline (VA-VAE) and highlights the benefit of frequency-aware modeling for learning more expressive, disentangled, and visually faithful latent embeddings. Notably, the performance gap between low and high-frequency reconstructions across all models highlights the general challenge of capturing fine details effectively.

Latent Generation Results

We evaluate the generative quality of our learned latent embeddings by training a diffusion-based generative model on top of the FA-VAE representations. Specifically, we use LightningDiT (Yao, Yang, and Wang 2025), a fast-converging latent diffusion backbone to model the generation process, and compare against a wide range of state-of-

the-art autoregressive and latent diffusion models, both with and without classifier-free guidance (CFG). Table 2 reports quantitative results across standard metrics: generation FID score (gFID), structural FID (sFID), Inception Score (IS), Precision, and Recall. Lower gFID and sFID values indicate better image fidelity and diversity, while higher IS, precision, and recall reflect better sample quality.

Table 2 shows comparison of LightningDiT with FA-VAE with other standard latent generation baselines. Our approach, **LightningDiT with FA-VAE**, achieves the best gFID among all methods, along with highly competitive sFID and strong scores across IS, precision, and recall with and without the CFG setting. Compared to auto-regressive models like MaskGIT (Chang et al. 2022), MAR (Li et al. 2024a), VAR (Tian et al. 2024), MagViT-v2 (Yu et al. 2023) and LlamaGen (Sun et al. 2024), as well as latent diffusion models such as MaskDiT (Zheng et al. 2023), DiT (Peebles and Xie 2023), SiT (Ma et al. 2024), FasterDiT (Yao et al. 2024), MDF (Gao et al. 2023) and REPA (Yu et al. 2024b), our method consistently delivers a better fidelity and diversity. Notably, it outperforms the LightningDiT baseline trained on VA-VAE embeddings across all metrics, demonstrating the advantage of our frequency-aware latent space in enhancing generation quality. These results validate the effectiveness of our FA-VAE framework for learning high-quality, structure-preserving representations that generalize well in generative pipelines. The qualitative results of our generated visualizations are shown in Figure 4.

Fairness in Latent Representations. We evaluate fairness in terms of how well the latent embeddings represent the complex categories within the dataset. An embedding space is considered fair if it enables faithful reconstructions across all data categories, particularly those that are structurally complex. Since these embeddings are used in the generation pipeline, under-representation of certain classes can result in biased or degraded outputs. To analyze this, we identify the top 100 ImageNet categories with the highest reconstruction error, measured by normalized recon-

Method	Tokenizer	Epochs	#Params	Generation w/o CFG					Generation w/ CFG				
				gFID	sFID	IS	Pre.	Rec.	gFID	sFID	IS	Pre.	Rec.
Autoregressive (AR)													
MaskGIT	VQ-VAE	555	227M	6.18	-	182.1	0.80	0.51	-	-	-	-	-
LlamaGen	VQ-VAE	300	3.1B	9.38	8.24	112.9	0.69	0.67	2.18	5.97	263.3	0.81	0.58
VAR	MS-VQ-VAE	350	2.0B	-	-	-	-	-	1.80	-	365.4	0.83	0.57
MagViT-v2	VQ-VAE	1080	307M	3.65	-	200.5	-	-	1.78	-	319.4	-	-
MAR	KL-VAE	800	945M	2.35	-	227.8	0.79	0.62	1.55	-	303.7	0.81	0.62
Latent Diffusion Models													
MaskDiT	SD-VAE	1600	675M	5.69	10.34	177.9	0.74	0.60	2.28	5.67	276.6	0.80	0.61
DiT	SD-VAE	1400	675M	9.62	6.85	121.5	0.67	0.67	2.27	4.60	278.2	0.83	0.57
SiT	SD-VAE	1400	675M	8.61	6.32	131.7	0.68	0.67	2.06	4.50	270.3	0.82	0.59
FasterDiT	SD-VAE	400	675M	7.91	5.45	131.3	0.67	0.69	2.03	4.63	264.0	0.81	0.60
MDT	SD-VAE	1300	675M	6.23	5.23	143.0	0.71	0.65	1.79	4.57	283.0	0.81	0.61
MDTv2	SD-VAE	1080	675M	-	-	-	-	-	1.58	4.52	314.7	0.79	0.65
REPA	SD-VAE	800	675M	5.90	-	-	-	-	1.42	4.70	305.7	0.80	0.65
LightningDiT	VA-VAE	64	675M	5.14	4.22	130.2	0.76	0.62	2.11	4.16	252.3	0.81	0.58
LightningDiT	FA-VAE	64	675M	3.24	4.09	193.7	0.83	0.69	1.32	4.07	317.4	0.83	0.65

Table 2: Comparison of generation performance of autoregressive and latent diffusion models with and without classifier-free guidance (CFG) vs LightningDiT with our FA-VAE tokenizer. Missing values are indicated by -. We report metrics only available in the respective works.

Model	Rec.	LF	HF	LPIPS	rFID
KL-VAE	0.1146	0.0645	0.1313	0.2151	0.7820
MS-VQ-VAE	0.0238	0.0705	0.0082	0.2331	0.8427
VA-VAE	0.0125	0.0263	0.0098	0.1071	0.6509
FA-VAE	0.0044	0.0114	0.0020	0.0940	0.4156

Table 3: Reconstruction comparison of tokenizers with input wavelet representation instead of input pixel representation. Rec.: Reconstruction Loss, LF: Low Frequency Loss, HF: High Frequency Loss. Lower is better.

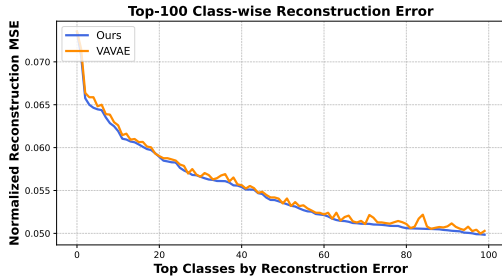


Figure 5: Top-100 classes by reconstruction error. Our model shows consistently lower MSE across challenging categories.

struction error using mean squared error (NMSE). Figure 5 presents the class-wise reconstruction loss performance on these challenging categories. Our frequency-aware model consistently achieves lower reconstruction errors compared to VA-VAE, indicating improved fidelity and robustness in capturing complex details. These results demonstrate that frequency-aware modeling facilitates more balanced and faithful reconstructions, particularly in high-error regions of the data distribution.

Ablation Study

To further investigate the contribution of decoupling low- and high-frequency components in our frequency-aware training strategy, we conduct an ablation study utilizing few latent embedding tokenizers from Table 1. Specifically, we retrain these models by coupling the low- and high-frequency components in a shared frequency space, using the same wavelet-based losses employed in our FA-VAE framework. In this setup, each tokenizer is optimized jointly on both low- and high-frequency representations obtained via the Discrete Wavelet Transform (DWT) using Haar filters. The results, presented in Table 3, demonstrate that our frequency-aware FA-VAE consistently outperforms the coupled-frequency variants across all metrics, including overall reconstruction error (Rec.), low-(LF) and high-frequency (HF) fidelity error, perceptual similarity loss (LPIPS), and reconstruction FID (rFID). This indicates that explicitly decoupling frequencies during training leads to more accurate and perceptually faithful reconstructions. For a fair comparison, all models are trained with similar latent dimensionality as used in the FA-VAE configuration.

Conclusion

In this work, we investigate frequency awareness in the latent embeddings of tokenizer models used within latent generative pipelines. We find that jointly optimizing low- and high-frequency components leads to a frequency bias favoring low-frequencies thereby degrading the reconstruction of fine-grained, high-frequency details and overall perceptual quality. To address this limitation, we introduce **FA-VAE**, a frequency-aware VAE framework that explicitly decouples low and high-frequency components via wavelet decomposition, processes them independently, and fuses them into a unified latent representation. FA-VAE achieves state-of-the-art performance across frequency-aware reconstruction metrics, demonstrating improved fidelity and perceptual quality.

References

- Bachmann, R.; Allardice, J.; Mizrahi, D.; Fini, E.; Kar, O. F.; Amirloo, E.; El-Nouby, A.; Zamir, A.; and Dehghan, A. 2025. FlexTok: Resampling Images into 1D Token Sequences of Flexible Length. In *Forty-second International Conference on Machine Learning*.
- Björk, S.; Myhre, J. N.; and Johansen, T. H. 2022. Simpler is better: Spectral regularization and up-sampling techniques for variational autoencoders. In *ICASSP 2022-2022 IEEE International Conference on Acoustics, Speech and Signal Processing (ICASSP)*, 3778–3782. IEEE.
- Blattmann, A.; Rombach, R.; Ling, H.; Dockhorn, T.; Kim, S. W.; Fidler, S.; and Kreis, K. 2023. Align your Latents: High-Resolution Video Synthesis with Latent Diffusion Models. In *Proc. CVPR 2023*.
- Chang, H.; Zhang, H.; Jiang, L.; Liu, C.; and Freeman, W. T. 2022. Maskgit: Masked generative image transformer. In *Proceedings of the IEEE/CVF Conference on Computer Vision and Pattern Recognition*, 11315–11325.
- Chen, H.; Han, Y.; Chen, F.; Li, X.; Wang, Y.; Wang, J.; Wang, Z.; Liu, Z.; Zou, D.; and Raj, B. 2025. Masked autoencoders are effective tokenizers for diffusion models. In *Forty-second International Conference on Machine Learning*.
- Chen, J.; Cai, H.; Chen, J.; Xie, E.; Yang, S.; Tang, H.; Li, M.; Lu, Y.; and Han, S. 2024. Deep compression autoencoder for efficient high-resolution diffusion models. *arXiv preprint arXiv:2410.10733*.
- Deng, J.; Dong, W.; Socher, R.; Li, L.-J.; Li, K.; and Fei-Fei, L. 2009. Imagenet: A large-scale hierarchical image database. In *2009 IEEE conference on computer vision and pattern recognition*, 248–255. Ieee.
- Dong, Y.; Zuo, Q.; Gu, X.; Yuan, W.; Zhao, Z.; Dong, Z.; Bo, L.; and Huang, Q. 2024. GPLD3D: Latent Diffusion of 3D Shape Generative Models by Enforcing Geometric and Physical Priors. In *Proc. CVPR 2024*, 56–66.
- Esser et al., P. e. a. 2021. Taming Transformers for High-Resolution Image Synthesis. In *Proceedings of the IEEE/CVF Conference on Computer Vision and Pattern Recognition (CVPR)*, 12873–12883.
- Gal, R.; Hochberg, D. C.; Bermanno, A.; and Cohen-Or, D. 2021. Swagan: A style-based wavelet-driven generative model. *ACM Transactions on Graphics (TOG)*, 40(4): 1–11.
- Gao, S.; Zhou, P.; Cheng, M.-M.; and Yan, S. 2023. Masked diffusion transformer is a strong image synthesizer. In *Proceedings of the IEEE/CVF International Conference on Computer Vision*, 23164–23173.
- Guth, F.; Coste, S.; De Bortoli, V.; and Mallat, S. 2022. Wavelet Score-Based Generative Modeling. In *NeurIPS*. Multi-scale diffusion over wavelet coefficients, linear time complexity.
- Heusel, M.; Ramsauer, H.; Unterthiner, T.; Nessler, B.; and Hochreiter, S. 2017. GANs trained by a two time-scale update rule converge to a local Nash equilibrium. In *Advances in Neural Information Processing Systems (NeurIPS)*, 6626–6637.
- Huang, L.; Fang, R.; Zhang, A.; Song, G.; Liu, S.; Liu, Y.; and Li, H. 2024. Fouriscale: A frequency perspective on training-free high-resolution image synthesis. In *European conference on computer vision*, 196–212. Springer.
- Huang, Z.; Qiu, X.; Ma, Y.; Zhou, Y.; Chen, J.; Zhang, H.; Zhang, C.; and Li, X. 2025. Nfig: Autoregressive image generation with next-frequency prediction. *arXiv preprint arXiv:2503.07076*.
- Hui, K.-H.; Sanghi, A.; Rampini, A.; Malekshan, K. R.; Liu, Z.; Shayani, H.; and Fu, C.-W. 2024. Make-a-shape: a ten-million-scale 3d shape model. In *Forty-first International Conference on Machine Learning*.
- Jiang, H.; Luo, A.; Fan, H.; Han, S.; and Liu, S. 2023. Low-light image enhancement with wavelet-based diffusion models. *ACM Transactions on Graphics (TOG)*, 42(6): 1–14.
- Jiang, L.; Dai, B.; Wu, W.; and Loy, C. C. 2021. Focal Frequency Loss for Image Reconstruction and Synthesis. In *Proceedings of the IEEE/CVF International Conference on Computer Vision (ICCV)*, 13919–13929.
- Karras, T.; Laine, S.; and Aila, T. 2019. A Style-Based Generator Architecture for Generative Adversarial Networks. In *CVPR*.
- Kim, C.; Moon, S. J.; and Park, G.-M. 2025. WINE: Wavelet-Guided GAN Inversion and Editing for High-Fidelity Refinement. In *2025 IEEE/CVF Winter Conference on Applications of Computer Vision (WACV)*, 4523–4532.
- Kim, Y.; Hwang, G.; Zhang, J.; and Park, E. 2025. Diffuse-high: Training-free progressive high-resolution image synthesis through structure guidance. In *Proceedings of the AAAI conference on artificial intelligence*, 4338–4346.
- Kingma, D. P.; and Welling, M. 2013. Auto-Encoding Variational Bayes. *arXiv preprint arXiv:1312.6114*.
- Kirillov, A.; Mintun, E.; Ravi, N.; Mao, H.; Rolland, L.; Gustafson, Y.; Xiao, C.-Y.; Whitehead, S.; et al. 2023. Segment Anything. *arXiv preprint arXiv:2304.02643*.
- Kouzelis, T.; Kakogeorgiou, I.; Gidaris, S.; and Komodakis, N. 2025. Eq-vae: Equivariance regularized latent space for improved generative image modeling. *arXiv preprint arXiv:2502.09509*.
- Krasin, I.; Duerig, T.; Alldrin, N.; Ferrari, V.; Abu-El-Haija, S.; Kuznetsova, A.; Rom, H.; Uijlings, J.; and et al. 2017. OpenImages: A public dataset for large-scale multi-label and multi-class image classification. *Dataset available from <https://storage.googleapis.com/openimages/web/index.html>*.
- Lee, D.; Kim, C.; Kim, S.; Cho, M.; and Han, W.-S. 2022. Autoregressive Image Generation Using Residual Quantization. In *Proceedings of the IEEE/CVF Conference on Computer Vision and Pattern Recognition (CVPR)*, 11523–11532.
- Li, T.; Tian, Y.; Li, H.; Deng, M.; and He, K. 2024a. Autoregressive Image Generation without Vector Quantization. *arXiv preprint arXiv:2406.11838*.
- Li, Y.; Zhao, H.; Zhou, J.; Xu, G.; Hu, T.; Chen, G.; and Wang, H. 2024b. FedSR: Frequency-Aware Enhancement for Diffusion-based Image Super-Resolution. In *ICLR 2025 (withdrawn)*. Amplitude and high-frequency enhancement modules for diffusion SR.

- Luo, S.; Tan, Y.; Huang, L.; Li, J.; and Zhao, H. 2024. Latent Consistency Models: Synthesizing High-Resolution Images with Few-Step Inference. In *Proc. ICLR 2024*.
- Ma, N.; Goldstein, M.; Albergo, M. S.; Boffi, N. M.; Vanden-Eijnden, E.; and Xie, S. 2024. Sit: Exploring flow and diffusion-based generative models with scalable interpolant transformers. *arXiv preprint arXiv:2401.08740*.
- Medi, T.; Rampini, A.; Reddy, P.; Jayaraman, P. K.; and Keuper, M. 2024a. 3D-WAG: Hierarchical Wavelet-Guided Autoregressive Generation for High-Fidelity 3D Shapes. *arXiv preprint arXiv:2411.19037*.
- Medi, T.; Tayyub, J.; Sarmad, M.; Lindseth, F.; and Keuper, M. 2024b. FullFormer: Generating Shapes Inside Shapes. In Köthe, U.; and Rother, C., eds., *Pattern Recognition*, 147–162. Cham: Springer Nature Switzerland. ISBN 978-3-031-54605-1.
- Miwa, K.; Sasaki, K.; Arai, H.; Takahashi, T.; and Yamaguchi, Y. 2025. One-d-piece: Image tokenizer meets quality-controllable compression. *arXiv preprint arXiv:2501.10064*.
- Mulcahy, C. 1997. Image compression using the Haar wavelet transform. *Spelman Science and Mathematics Journal*, 1(1): 22–31.
- Neuhof, G.; Ollmann, T.; Rota Bulò, S.; and Kotschieder, P. 2017. The Mapillary Vistas Dataset for Semantic Understanding of Street Scenes. In *ICCV*.
- Oquab, M.; Darcet, T.; Moutakanni, T.; Vo, H.; Szafraniec, M.; Khalidov, V.; Fernandez, P.; Haziza, D.; Massa, F.; El-Nouby, A.; et al. 2023. Dinov2: Learning robust visual features without supervision. *arXiv preprint arXiv:2304.07193*.
- Peebles, W.; and Xie, S. 2023. Scalable diffusion models with transformers. In *Proceedings of the IEEE/CVF International Conference on Computer Vision*, 4195–4205.
- Phung, H.; Dao, Q.; and Tran, A. 2023. Wavelet Diffusion Models Are Fast and Scalable Image Generators. In *Proceedings of the IEEE/CVF Conference on Computer Vision and Pattern Recognition (CVPR)*, 10199–10208.
- Qian, Y.; Cai, Q.; Pan, Y.; Li, Y.; Yao, T.; Sun, Q.; and Mei, T. 2024. Boosting diffusion models with moving average sampling in frequency domain. In *Proceedings of the IEEE/CVF conference on computer vision and pattern recognition*, 8911–8920.
- Rombach, R.; Blattmann, A.; Lorenz, D.; Esser, P.; and Ommer, B. 2022. High-Resolution Image Synthesis With Latent Diffusion Models. In *Proceedings of the IEEE/CVF Conference on Computer Vision and Pattern Recognition (CVPR)*, 10684–10695.
- Skorokhodov, I.; Girish, S.; Hu, B.; Menapace, W.; Li, Y.; Abdal, R.; Tulyakov, S.; and Siarohin, A. 2025. Improving the diffusability of autoencoders. *arXiv preprint arXiv:2502.14831*.
- Sun, P.; Jiang, Y.; Chen, S.; Zhang, S.; Peng, B.; Luo, P.; and Yuan, Z. 2024. Autoregressive Model Beats Diffusion: Llama for Scalable Image Generation. *arXiv preprint arXiv:2406.06525*.
- Szegedy, C.; Vanhoucke, V.; Ioffe, S.; Shlens, J.; and Wojna, Z. 2016. Rethinking the inception architecture for computer vision. In *Proceedings of the IEEE Conference on Computer Vision and Pattern Recognition (CVPR)*, 2818–2826.
- Takida, Y.; Ikemiya, Y.; Shibuya, T.; Shimada, K.; Choi, W.; Lai, C.-H.; Murata, N.; Uesaka, T.; Uchida, K.; Liao, W.-H.; et al. 2023. Hq-vae: Hierarchical discrete representation learning with variational bayes. *arXiv preprint arXiv:2401.00365*.
- Tian, K.; Jiang, Y.; Yuan, Z.; Peng, B.; and Wang, L. 2024. Visual Autoregressive Modeling: Scalable Image Generation via Next-Scale Prediction. In *Advances in Neural Information Processing Systems*, volume 37, 84839–84865.
- Vahdat, A.; and Kautz, J. 2020. NVAE: A Deep Hierarchical Variational Autoencoder. In *Neural Information Processing Systems (NeurIPS)*.
- Van Den Oord, A.; Vinyals, O.; et al. 2017. Neural discrete representation learning. *Advances in neural information processing systems*, 30.
- Xie, E.; Chen, J.; Chen, J.; Cai, H.; Tang, H.; Lin, Y.; Zhang, Z.; Li, M.; Zhu, L.; Lu, Y.; and Han, S. 2024. Sana: Efficient High-Resolution Image Synthesis with Linear Diffusion Transformer. *arXiv:2410.10629*.
- Xie, E.; Chen, J.; Zhao, Y.; Yu, J.; Zhu, L.; Lin, Y.; Zhang, Z.; Li, M.; Chen, J.; Cai, H.; et al. 2025. SANA 1.5: Efficient Scaling of Training-Time and Inference-Time Compute in Linear Diffusion Transformer. *arXiv:2501.18427*.
- Xu, W.; Yue, X.; Wang, Z.; Teng, Y.; Zhang, W.; Liu, X.; Zhou, L.; Ouyang, W.; and Bai, L. 2025. Exploring representation-aligned latent space for better generation. *arXiv preprint arXiv:2502.00359*.
- Yang, X.; Zhou, D.; Feng, J.; and Wang, X. 2023. Diffusion probabilistic model made slim. In *Proceedings of the IEEE/CVF Conference on computer vision and pattern recognition*, 22552–22562.
- Yao, J.; Cheng, W.; Liu, W.; and Wang, X. 2024. FasterDiT: Towards Faster Diffusion Transformers Training without Architecture Modification. *arXiv preprint arXiv:2410.10356*.
- Yao, J.; Yang, B.; and Wang, X. 2025. Reconstruction vs. generation: Taming optimization dilemma in latent diffusion models. In *Proceedings of the IEEE/CVF Conference on Computer Vision and Pattern Recognition*.
- Yu, L.; Lezama, J.; Gundavarapu, N. B.; Versari, L.; Sohn, K.; Minnen, D.; Cheng, Y.; Birodkar, V.; Gupta, A.; Gu, X.; et al. 2023. Language Model Beats Diffusion–Tokenizer is Key to Visual Generation. *arXiv preprint arXiv:2310.05737*.
- Yu, Q.; Weber, M.; Deng, X.; Shen, X.; Cremers, D.; and Chen, L.-C. 2024a. An Image is Worth 32 Tokens for Reconstruction and Generation. In *Advances in Neural Information Processing Systems*, volume 37, 128940–128966.
- Yu, S.; Kwak, S.; Jang, H.; Jeong, J.; Huang, J.; Shin, J.; and Xie, S. 2024b. Representation Alignment for Generation: Training Diffusion Transformers Is Easier Than You Think. *arXiv preprint arXiv:2410.06940*.

- Yu, Y.; Zhan, F.; Lu, S.; Pan, J.; Ma, F.; Xie, X.; and Miao, C. 2021. WaveFill: A Wavelet-Based Generation Network for Image Inpainting. In *Proceedings of the IEEE/CVF International Conference on Computer Vision (ICCV)*, 14114–14123.
- Yuan, X.; Li, L.; Wang, J.; Yang, Z.; Lin, K.; Liu, Z.; and Wang, L. 2023. Spatial-frequency u-net for denoising diffusion probabilistic models. *arXiv preprint arXiv:2307.14648*.
- Zhang, J.; Huang, Q.; Liu, J.; Guo, X.; and Huang, D. 2025. Diffusion-4K: Ultra-High-Resolution Image Synthesis with Latent Diffusion Models. In *Proceedings of the Computer Vision and Pattern Recognition Conference (CVPR)*, 23464–23473.
- Zhang, R.; Isola, P.; Efros, A. A.; Shechtman, E.; and Wang, O. 2018. The unreasonable effectiveness of deep features as a perceptual metric. In *Proceedings of the IEEE Conference on Computer Vision and Pattern Recognition (CVPR)*, 586–595.
- Zhao, C.; Cai, W.; Dong, C.; and Hu, C. 2024. Wavelet-based fourier information interaction with frequency diffusion adjustment for underwater image restoration. In *Proceedings of the IEEE/CVF Conference on Computer Vision and Pattern Recognition*, 8281–8291.
- Zheng, H.; Nie, W.; Vahdat, A.; and Anandkumar, A. 2023. Fast training of diffusion models with masked transformers. *arXiv preprint arXiv:2306.09305*.
- Zhou, C.; Wang, X.; and Zhang, M. 2024. Unifying Generation and Prediction on Graphs with Latent Graph Diffusion. In *Proc. NeurIPS 2024*.

Appendix

In this appendix, we provide additional details supporting our main paper. The sections below elaborate on the architectural design, implementation specifics, and qualitative visualizations that complement our experimental findings:

- ✓ Architectural details of FA-VAE
- ✓ Implementation specifics and training setup
- ✓ Visualization comparisons highlighting reconstruction quality
- ✓ Additional Experiments

Architectural Details of FA-VAE

The architecture of our Frequency-Aware Variational Autoencoder (FA-VAE) consists of two independent encoder-decoder pairs, designed to separately process low- and high-frequency components of the input data. The encoder-decoder architecture is inspired by standard VAE setups.

Shared Architectural Design

Each encoder and decoder follows a symmetric U-Net-style architecture with hierarchical multiscale processing. The core building blocks are `ResnetBlocks` with group normalization and Swish activations. Attention modules (`AttnBlock` or `LinearAttention`) are interleaved based on spatial resolution thresholds to capture long-range dependencies, particularly at intermediate scales such as 8×8 or 16×16 . Downsampling in the encoder is performed via strided convolutional layers or average pooling, while upsampling in the decoder uses nearest-neighbor interpolation followed by convolution. The spatial resolution halves at each stage, yielding a compact bottleneck latent representation. This architectural design for individual encoder-decoder setup is inherited from (Li et al. 2024a).

Low- and High-Frequency Encoding

To enable frequency-aware modeling, the input is first decomposed using the discrete wavelet transform (DWT) with a Haar filter at **level 1 decomposition**, yielding a low-frequency component (LL) and high-frequency components (LH, HL, HH). These frequency components are then processed separately:

- **Low-Frequency Encoder:** This encoder receives the LL component and maps it through a standard hierarchical structure, outputting the parameters (mean and log-variance) of a diagonal Gaussian distribution. These parameters define the variational posterior from which low-frequency latent codes are sampled.
- **High-Frequency Encoder:** The high-frequency tensor is reshaped and passed through a parallel encoder, similar in design to the low-frequency branch but adapted for higher input dimensionality (i.e., 9 channels for 3 scales \times 3 orientations of LH, HL, HH). It also outputs Gaussian parameters and samples latent variables accordingly.

Both encoders use the `MergedRescaleEncoder` module, which applies additional residual blocks and attention after the initial latent encoding, allowing controlled compression and modulation of spatial structure.

Bottleneck and Latent Space

Each encoder produces a bottleneck representation at a spatial scale determined by the number of downsampling layers (typically 16×16 or 8×8), with a corresponding increase in channel dimensionality. The encoder outputs are passed through 1×1 convolutional layers to double the channels and parameterize a Gaussian distribution, following the VAE formulation (Van Den Oord, Vinyals et al. 2017). Sampling is performed using the reparameterization trick.

Decoding and Reconstruction

The sampled latent codes are passed through their respective decoders, which reverse the hierarchy of the encoder. The decoder structure mirrors the encoder in terms of resolution levels and attention placement. The outputs from the low- and high-frequency decoders are projected back to image space using a wavelet inversion step using inverse DWT.

Hierarchical Extensions

To improve semantic alignment and generalization, FA-VAE, inspired from VA-VAE (Yao, Yang, and Wang 2025) integrates the `FirstStagePostProcessor`, which enables conditioning on external features from a pretrained model (Dinov2). These modules enhance the latent space with multiscale guidance. This module is only active for low frequency encoded latents. During Generation, we model the concatenated low and high frequency latent embeddings using `LightningDit` (Yao, Yang, and Wang 2025). There are no architectural changes during the generation pipeline and only minimal adjustments in the auto-encoding pipeline.

Implementation Details

We follow a similar hyperparameter setup to (Rombach et al. 2022; Yao, Yang, and Wang 2025) for implementing our latent reconstruction and generation pipeline. For the visual tokenizer, we adopt the architectural backbone and training scheme from LDM (Rombach et al. 2022; Li et al. 2024a), leveraging a VQGAN-style encoder-decoder structure but omitting quantization to obtain a continuous latent space regulated by KL divergence. We apply the KL loss directly over the latent representation as in (Yao, Yang, and Wang 2025). To support distributed training across multiple nodes, we scale the learning rate and global batch size to 1×10^{-4} and 256, respectively, following the MAR setup (Li et al. 2024a). We experiment with two different $f16$ tokenizers: one trained without alignment for high frequencies and one with VF loss using DINOv2 (Oquab et al. 2023) for low frequencies. Here, f represents the spatial resolution factor and d the latent feature dimensionality. Following (Yao, Yang, and Wang 2025), we set the VF loss hyperparameters to $m_1 = 0.5$, $m_2 = 0.25$, and $w_{\text{hyper}} = 0.1$.

For generative modeling, we employ `LightningDiT` (Yao, Yang, and Wang 2025), incorporating architectural enhancements and training strategies outlined in their work. The latent features extracted from the FA-VAE tokenizer are used to train `LightningDiT` models on ImageNet at 256×256 resolution for 64 epochs. The patch size is set to 1 to ensure the effective downsampling rate of the entire system

Model	Tokenizer Config	Recon. Loss	Low Freq. Loss	High Freq. Loss	LPIPS
DC-AE*	f32c32	0.0213	0.0521	0.0110	0.1708
DC-AE*	f32c32	0.0197	0.0478	0.0103	0.1704
DC-AE*	f64c128	0.0206	0.0499	0.0109	0.1689
DC-AE*	f128c512	0.0208	0.0510	0.0107	0.1756
KL-VAE [†]	f4c3	0.0064	0.0097	0.0053	0.0722
KL-VAE [†]	f8c4	0.0156	0.0348	0.0091	0.1459
KL-VAE [†]	f16c16	0.0163	0.0365	0.0096	0.1529
KL-VAE [†]	f32c64	0.0251	0.0640	0.0121	0.2089
KL-VAE [†]	f64c128	0.0241	0.0652	0.0105	0.1708
VQ-VAE [†]	f4c3v8192	0.0064	0.0104	0.0051	0.0693
VQ-VAE [†]	f8c4v16384	0.0203	0.0475	0.0113	0.1701
VQ-VAE [†]	f8c4v256	0.0239	0.0569	0.0128	0.1848
VQ-VAE [†]	f16c8v16384	0.0352	0.1006	0.0134	0.2637
KL-VAE [‡]	f8c4 (ema)	0.0145	0.0313	0.0089	0.1345
FA-VAE (Ours)	f16c32	0.0044	0.0114	0.0020	0.0940

Table 4: Comparison of tokenizers on the ImageNet validation set across frequency-aware and perceptual metrics. Lower values indicate better performance. **f** denotes the latent spatial downsampling factor (e.g., $f=16$ implies $16\times$ downsampling in width and height), and **c** denotes the number of latent channels. For VQ models, **v** indicates the vocabulary size. * Models trained on ImageNet, SAM, FFHQ, and Mapillary Vistas. [†] Models trained on OpenImages. [‡] Models fine-tuned on OpenImages and LAION.

remains at 16, aligning with the approach in (Chen et al. 2024). We trained our models using 4 H100 Nvidia GPUs with 93.58GB VRAM.

Explanation of Metrics. We report several standard metrics commonly used to evaluate the quality of generated images from autoregressive and latent diffusion models.

- **gFID** (generation FID): Frechet Inception Distance computed between generated images and real images, using the Inception-v3 network. Lower values indicate better alignment in feature distributions and overall visual fidelity.
- **sFID** (spatial FID): A structural or spatial-aware variant of FID. sFID is equivalent to FID but uses intermediate spatial features in the inception network rather than the spatially-pooled features used in standard FID.
- **IS** (Inception Score): Measures both the confidence and diversity of generated images based on class predictions from the Inception network. Higher IS indicates better generative diversity and visual sharpness.
- **Precision (Pre.) and Recall (Rec.):** These metrics assess the coverage and fidelity of the generated data manifold with respect to real images. Higher precision implies fewer unrealistic samples (fidelity), while higher recall indicates better diversity and coverage.

All metrics are computed using 50K generated samples. We report results both **with** and **without Classifier-Free Guidance (CFG)** when available, which is a commonly used sampling technique in diffusion models to improve sample quality. Missing entries (marked as –) reflect the unavailability of results in the respective original papers.

Visualization Comparisons

We qualitatively visualize the reconstructions of the best three models from Table 1 in the main paper, namely **FA-**

VAE (Ours), **KL-VAE**, and **VA-VAE**, selected based on their overall lowest reconstruction losses. These models represent a diverse set of tokenizers with similar latent spatial compression and achieve top-tier quantitative performance across both reconstruction and perceptual metrics. Without cherry-picking, we present their reconstructions to highlight the perceptual fidelity of **FA-VAE** compared to the best-performing baselines.

As shown in Figures 6, 7, and 8, FA-VAE achieves superior visual quality and preserves fine details better than KL-VAE and VA-VAE.

Additional Evaluations

To evaluate the reconstruction capabilities and perceptual fidelity of different tokenizer models trained on larger datasets, we report in Table 4 a comparison across frequency-aware metrics (reconstruction, low/high frequency loss) and LPIPS perceptual similarity on the ImageNet (Deng et al. 2009) validation set. Our proposed **FA-VAE** achieves the best performance across all frequency bands and ranks competitively in perceptual similarity, outperforming prior models such as KL-VAE[†] and VQ-VAE[†] trained on OpenImages (Krasin et al. 2017), as well as DC-AE* trained on broader multi-domain datasets (ImageNet (Deng et al. 2009), SAM (Kirillov et al. 2023), FFHQ (Karras, Laine, and Aila 2019), Mapillary Vistas (Neuhold et al. 2017)). These results underscore the effectiveness of frequency-aware latent representations in capturing high perceptual details. We believe our method, if trained on larger datasets, would exhibit even more beneficial results.

The DC-AE, KL-VAE, and VQ-VAE architectures and training setups are adapted from prior work (Xie et al. 2024, 2025; Rombach et al. 2022).

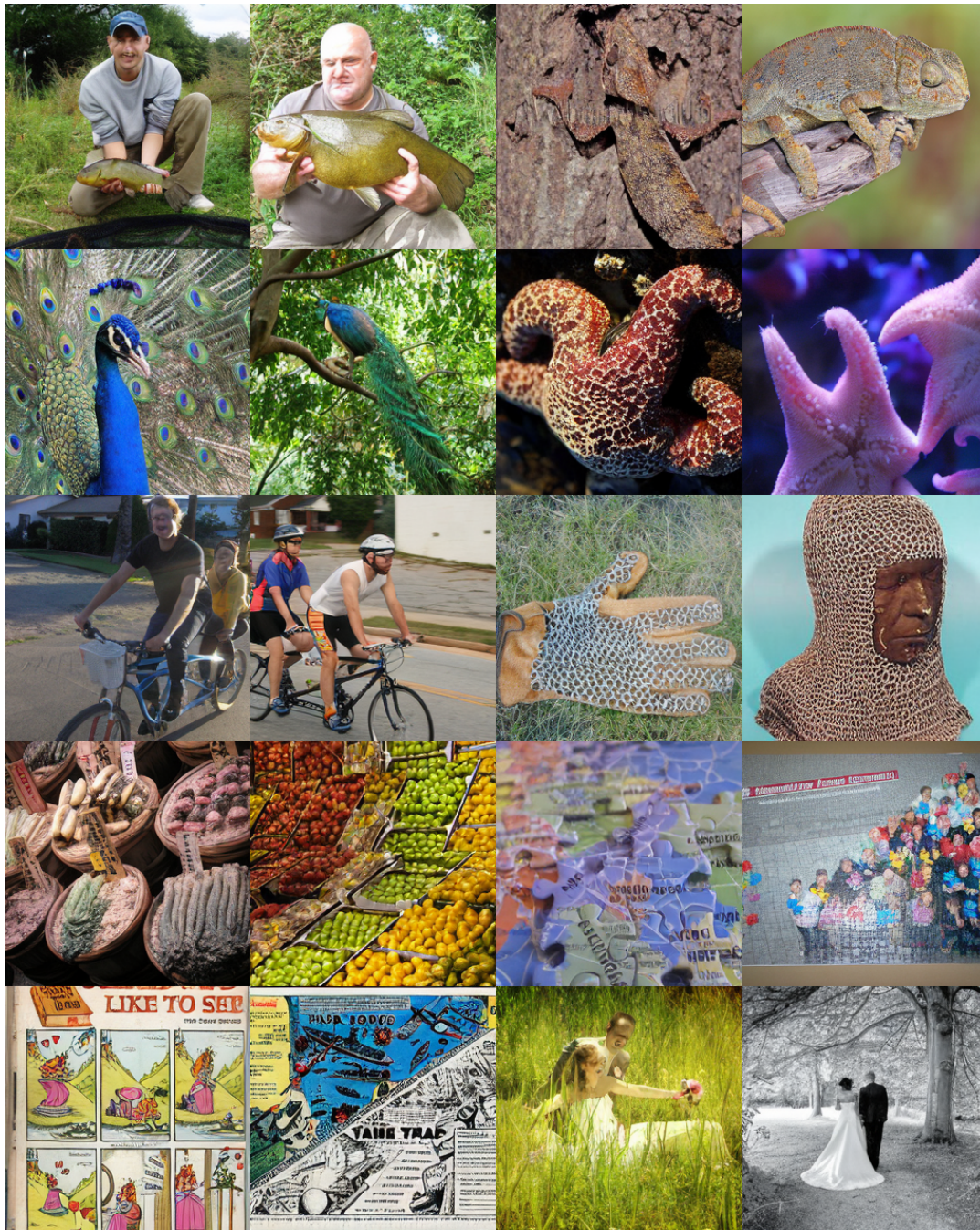


Figure 6: Qualitative reconstructions using **KL-VAE** on ImageNet 256×256 .



Figure 7: Qualitative reconstructions using VA-VAE on ImageNet 256×256 .

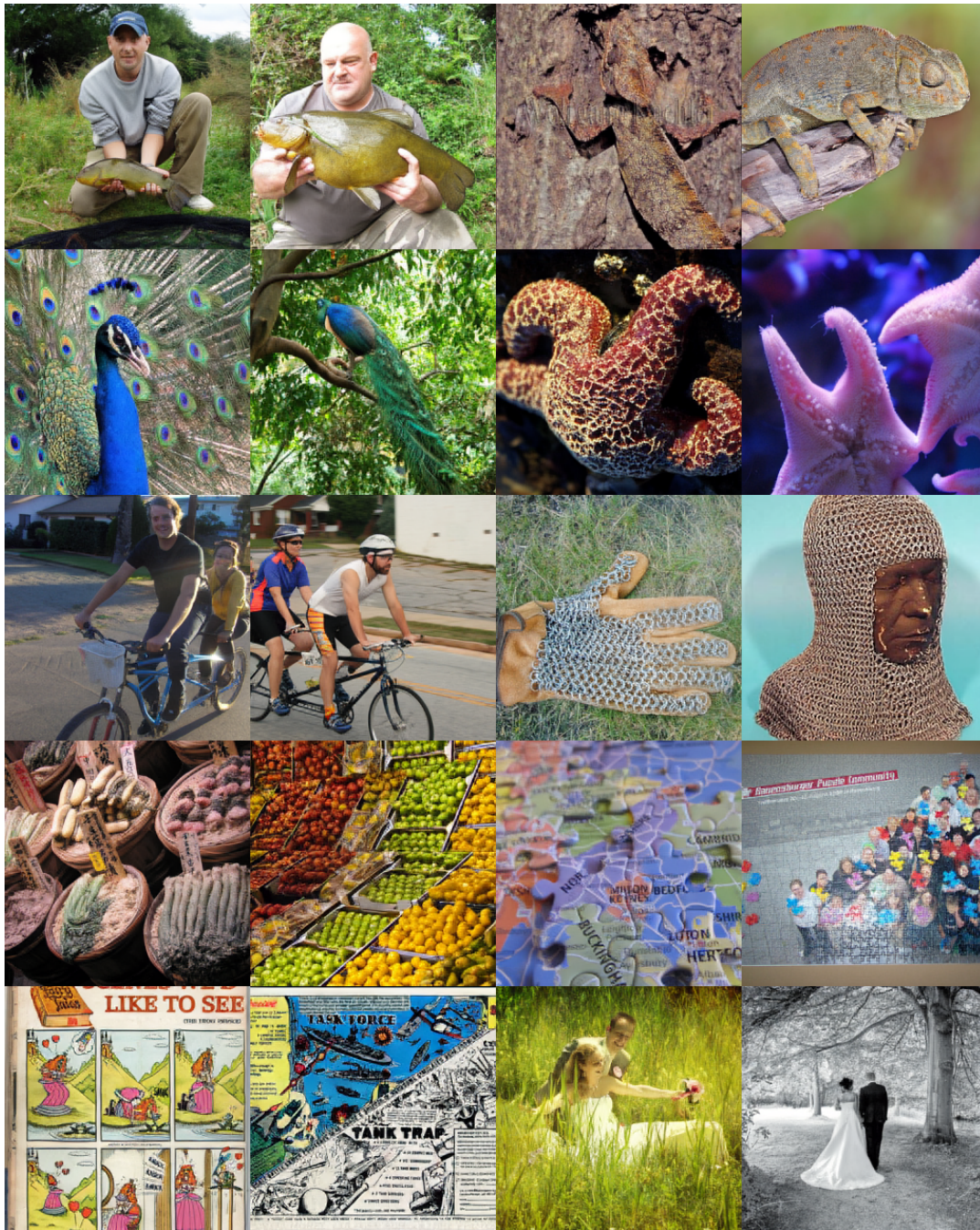


Figure 8: Qualitative reconstructions using our proposed **FA-VAE** on ImageNet 256×256 .